Response of a novel all-solid-state sodium-based-electrolyte battery to quasi-static and dynamic stimuli

Bruno G Christoff[1] (iD), Denys Marques[2,3], Maísa M Maciel[3] (iD),
Pouria Ataabadi[4], João Carmo[5], Maria H Braga[6,7], Rui M Guedes[1,7],
Marcílio Alves[4] and Volnei Tita[1,3] (iD)

Abstract

In response to growing environmental and economic concerns, developing new technologies prioritising safety, sustainability, and reliability has become imperative. In the energy sector, batteries play an increasingly significant role in applications such as powering electronic devices and vehicles. In this context, lithium-ion batteries have raised environmental concerns, driving the exploration of alternative technologies. Sodium-based batteries have emerged as an attractive option due to their environmental and economic advantages, as well as their potential for multi-functional applications. This study investigates a novel battery developed by a research team at the University of Porto, with a specific focus on its strain-sensing capabilities for potential applications in damage detection of structures. The battery under investigation is a novel all-solid-state design, comprised of a sodium-ion ferroelectric electrolyte and zinc and copper as the negative and positive electrodes, respectively. A series of quasi-static and dynamic tests are conducted to qualitatively assess the piezo-electric behaviour of the battery. The consistent findings show that the battery generates a difference in the electric potential in response to mechanical stimuli, thus confirming its piezoelectric nature. Furthermore, the results demonstrate the battery can accurately detect the operating frequencies of a shaker, despite encountering inherent electromagnetic interference noise from the electrical grid during testing. These promising outcomes highlight the substantial potential of this emerging technology for a wide range of applications, including but not limited to structural health monitoring systems. Given its novelty, this technology presents multi-functional capabilities for diverse practical future applications, such as energy harvesting that leads to self-powered structural health monitoring systems.

Keywords

Novel piezoelectric battery, sensing capabilities, multi-functional battery, structural health monitoring

Introduction

The escalating global population growth presents a series of challenges related to global warming, energy production, and energy storage.[1] This demographic expansion places increasing demands on energy production and storage, all while minimising CO_2 emissions.[2]

Batteries have found extensive applications in powering diverse devices, including cars and electronic gadgets.[3] In response to environmental concerns, the development of new technologies now emphasises not only the reliability, low cost, and high energy density of batteries but also eco-friendly materials and processes.[4,5] Meeting the energy needs of an ever-growing global society while ensuring sustainability has become an urgent priority.[3] Environmental considerations concerning batteries have been a long-standing issue, with sustainability now considered an additional design variable alongside structure,

[1]Department of Mechanical Engineering, Faculty of Engineering of the University of Porto, Porto, Portugal
[2]Department of Mechanical Engineering, Federal Center of Technological Education Celso Suckow da Fonseca, Angra dos Reis, RJ, Brazil
[3]Department of Aeronautical Engineering, São Carlos School of Engineering, University of São Paulo, São Carlos, SP, Brazil
[4]Department of Mechatronics and Mechanical Systems Engineering, Engineering School of the University of São Paulo, University of São Paulo, São Paulo, SP, Brazil
[5]Department of Electrical Engineering, São Carlos School of Engineering, University of São Paulo, São Carlos, SP, Brazil
[6]Department of Engineering Physics, Faculty of Engineering, University of Porto, Porto, Portugal
[7]LAETA - INEGI, Institute of Science and Innovation in Mechanical and Industrial Engineering, Porto, Portugal

Corresponding author:
Bruno G Christoff, Department of Mechanical Engineering, Faculty of Engineering of the University of Porto, Porto, Portugal.
Email: bchristoff@fe.up.pt

composition, and morphology in the development of new materials.[2]

The development, production, and use of environmentally friendly batteries are vital to meet the increasing energy demand in an eco-friendly and sustainable manner. This is particularly important in the context of a future climate-neutral economy with a zero-emission mobility goal.[6–8]

Lithium-ion batteries (LIBs) currently dominate various markets, powering electronic devices, electric vehicles, and more.[9] LIBs offer exceptional performance in terms of energy density[3,10–14] and have demonstrated high energy and power density, as well as long life.[4,15] However, LIBs suffer from limitations such as slow charging, the flammability of their electrolytes, and cathodes approaching their theoretical capacity limits.[6,16] Additionally, their usage and manufacturing have some drawbacks, including safety concerns associated with flammable electrolytes and limited usability in high-temperature environments.[2]

Another significant challenge is the high cost and limited availability of lithium resources,[6,10] hindering the widespread adoption of LIBs, particularly in large-scale energy storage applications.[9] Development of alternative technologies with better performance and economic advantages is crucial to meet the growing demand for renewable energy storage while reducing costs.[3,11,17]

As an alternative to LIBs, solid-state electrolytes (SSEs) have gained attention due to advantages like non-flammability, leak-proof nature, and improved mechanical properties.[18,4] The latter feature makes SSEs particularly interesting for structural battery applications. Among SSEs, Sodium-ion batteries (NIBs) closely resemble the well-established LIBs.[19] Sodium and lithium, both alkali metals, share similar chemical properties, resulting in identical fundamental principles.[10] NIBs are considered the next-generation of batteries,[9] offering improved thermal and chemical stability, reduced flammability, and enhanced durability due to their SSEs compared to conventional liquid organic electrolytes.[20,21] Another critical advantage of NIBs is the abundance of sodium in Earth's crust, which reduces production costs compared to LIBs.[22,6] Furthermore, NIBs, which do not require conventional cathodes and anodes, are well-suited for structural battery applications[6,15,23]

Moreover, several authors have emphasised the importance of developing autonomous structural health monitoring (SHM) systems with self-powering capabilities through the use of piezoelectric transducers.[24–26] However, the process of harvesting and converting mechanical energy may not provide sufficient power to fully sustain an SHM system,[27–29] making them still dependent on an external power source like batteries. Given the scenario described, the importance of developing autonomous SHM systems with self-powering capabilities becomes evident. Therefore, various scientific contributions focused on developing new concepts for multifunctional batteries. Notably, researchers at the Faculty of Engineering of the University of Porto (FEUP – Portugal) have introduced a battery constructed from multifunctional materials.[15] The

research team at FEUP has developed solid-state ferroelectric electrolytes, serving as the core component of these novel batteries. This intrinsic property implies that the electrolyte possesses piezoelectric characteristics, indicating substantial potential for use as a structural damage sensor in SHM systems.[30]

Considering the environmental and economic factors and the potential use of NIBs as structural batteries and as a sensor for SHM systems, this technology holds great promise for various engineering applications, including vehicles, drones, aircraft, etc. NIB adoption could lead to more efficient and eco-friendly energy storage alternatives, potentially reducing the weight, volume, and energy consumption of electric vehicles and devices.[15]

Hence, this study aims to understand the functionality of batteries developed at the University of Porto and demonstrate for the first time its piezoelectric response with a focus on their future potential applicability in SHM of composite structures. To achieve this, quasi-static and dynamic tests are performed on these batteries to assess their electrical response under these test conditions. It is important to note that the primary interest in these tests is to gain qualitative insights into the electrical behaviour of the batteries. Consequently, this work serves as a proof-of-concept, demonstrating the potential use of this emerging technology in future applications as a sensor.

Experimental procedure

The electrical response of the battery is assessed under quasi-static and dynamic stimuli. In the present tests, it is very important to highlight that the battery was not attached to any other structures that could be monitored by the battery itself. The response of the battery was investigated by applying quasi-static or dynamic stimuli directly to the battery. For the quasi-static tests, an experimental setup has been designed, in which the battery is positioned between two flat surfaces to better distribute the loading on the effective area of the battery. The loading is applied both manually and by placing a known weight on the battery. The signal generated by the battery is read by an oscilloscope. For the dynamic tests, the battery is directly attached to an electrodynamic shaker. The shaker's base excitation is transmitted to the battery under predefined constant sine wave frequency and as sweep sine waves. As the battery is ferroelectric, one expects to observe an electrical potential difference when the battery is subjected to mechanical deformation.

The battery

The battery utilised in this study is a novel all-solid-state structural battery developed by a research team at the University of Porto, Portugal.[4] This battery comprises a ferroelectric electrolyte based on sodium-ion ($Na_{2.99}Ba_{0.005}ClO$) and employs a zinc ($-$) and copper ($+$) electrode pair, as illustrated in Figure 1(a).

Furthermore, the battery features a protective polymeric film coating, as demonstrated in Figure 1(b). This
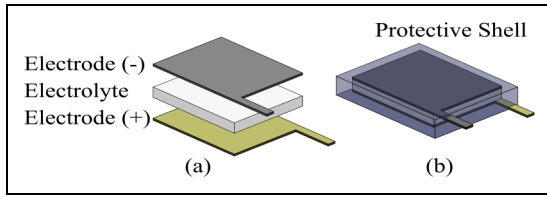
Figure 1. Schematics of the all-solid-state battery: (a) Electrodes (zinc (−) and copper (+)) and sodium-based electrolyte; (b) battery assembly and protective polymeric shell.

Figure 2. The battery and a voltage reading.

coating shields the electrolyte from potential atmospheric contact to detour adverse chemical reactions. Figure 2 shows one of the batteries used in the experiments and a voltage measurement for illustration. The functional part of the battery is seen in this picture, embedded in the polymeric coating. Hence, the lifespan is intricately connected to the lifespan of the protective film. If the polymeric film deteriorates, the battery is also susceptible to failure. Conversely, the thinness of the film ensures minimal impact on the battery's behaviour. The battery consists of a single cell with an effective surface area of 2×2 cm^2, and the electrolyte is impregnated on a cellulose membrane with a total thickness of 1 mm. The open circuit voltage of the fully charged cell was 1.0 V.

The battery incorporates a ferroelectric electrolyte, characterised by its spontaneous polarisation, belonging to the category of dielectric materials. Ferroelectric materials form a distinct subset that encompasses piezoelectric, pyroelectric, and dielectric properties. Specifically, materials categorised as ferroelectric must also exhibit pyroelectric, piezoelectric, and dielectric characteristics, with the broader classification following the hierarchy: dielectric > piezoelectric > pyroelectric > ferroelectric.

In addition to the properties detailed in this context, the specific ferroelectric electrolyte, $Na_{2.99}Ba_{0.005}ClO$, demonstrates noteworthy ferroelectric qualities as outlined in Carvalho Baptista et al.[4] Consequently, given the inherent piezoelectric properties within the battery, it is expected that the battery produces a potential difference under mechanical deformation.

Quasi-static testing

The initial tests consist of subjecting the battery to static or quasi-static loads. In these experiments, the goal is to observe changes in the electrical potential generated by the battery due to these loads. Figure 3 schematically illustrates the static test considered.

Since the battery has a slightly irregular surface, it is positioned on a flat stationary base. Additionally, to ensure a more uniform distribution of loads on the battery, another flat surface is placed over it. Two methods of applying quasi-static loads are considered for this test. In the first method, the load is applied manually to the battery, with no control over the applied load level. In the second method, a weight with a known mass is placed on the battery. It is worth noting that the
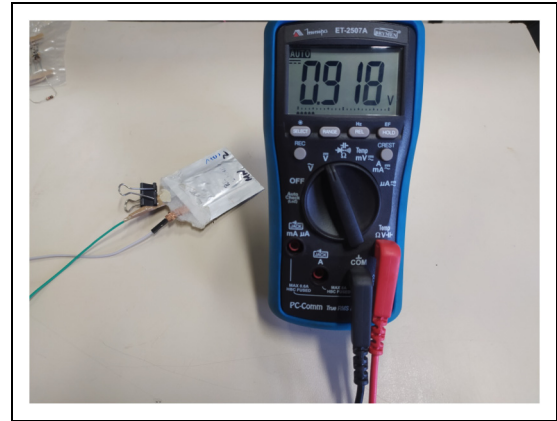
objective is to verify if there is a piezoelectric response in the battery, rather than quantifying the effect. In both cases, the load is applied in the *z*-direction (Figure 3), i.e., in the direction of electrodes and electrolyte stacking.

Electrical connections directly linked to the external parts of the battery electrodes (see Figure 1(b)), transmit the battery signal to a simple circuit mounted on a breadboard. This circuit is designed to filter out the DC component from the battery while allowing the passage of voltage oscillations induced by perturbations in the battery. The signal is read by an oscilloscope (Keysight DSOC1204A) and recorded in a text file format for post-processing.

Dynamic testing

Dynamic tests are also considered to assess the potential use of the battery as a strain-sensing device. In this scenario, the battery is subjected to dynamic loads under controlled frequencies, and the potential difference generated by the battery under these conditions is examined. The schematic of the experimental setup is shown in Figure 4.

An arbitrary function generator (AFG) (Minipa MFG-4205C) is configured to produce controlled and well-defined wave functions, which are then directly utilised to induce vibrations in an electrodynamic shaker (VEB Robotron-Meßelektronik 'Otto Schön'). Additionally, the AFG is set to generate a variety of constant sine-wave frequencies, as well as sweep-like excitations, allowing the investigation of the battery's behaviour under different scenarios. In all cases, a peak-to-peak voltage (V_{pp}) of 10 V is applied, corresponding to the maximum output voltage of the AFG.

The electric signal from the AFG is transformed into mechanical excitation by the electrodynamic shaker at the same frequency as the input signal. This dynamic mechanical displacement is then transmitted to a rigid grip designed to function as a clamping device for the battery. Two configurations are considered for attaching the battery to the rigid grip. In the first scenario, the entire effective area of the battery (including electrodes and the electrolyte) is enclosed within the rigid grip. In the second scenario, the effective area of the battery extends beyond the grip, and the polymeric protection is
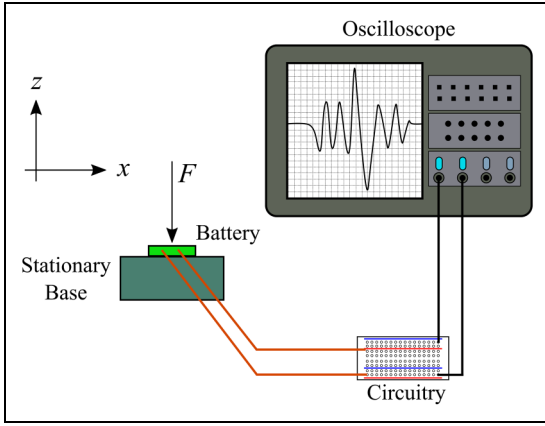
Figure 3. Static test setup. The battery is placed on a stationary base, and a force is applied. The signal passes through an electrical circuit, which is then read by the oscilloscope.
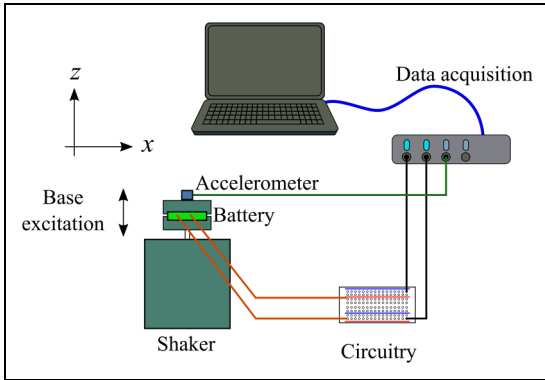

Figure 4. Dynamic test setup. The battery is attached directly to the electrodynamic shaker, and a known base excitation is applied. The signal is then routed through an electrical circuit, followed by a data acquisition system, and finally sent to the computer for data processing.

attached to the rigid grip, resulting in a condition similar to a cantilever beam.

Electrical connections directly linked to the external parts of the battery electrodes (Figure 1(b)) transmit the generated electrical signal from the battery to a simple circuit mounted directly on a breadboard, designed to remove its DC output voltage while allowing the passage of the voltage oscillations expected to happen during the vibration tests. For comparison, an accelerometer (Miniature PiezoBeam Accelerometer Kistler 500 mV/g type 8640A10) is attached to the rigid grip to guarantee that the battery generates a signal in the same frequency as the base excitation. Both the electrical voltage from the battery and the accelerometer signal are measured by a Kistler LabAmp 5167A data acquisition system and recorded in a computer for post-processing.

The circuitry

Figure 5 schematically depicts the electronic circuit utilised to filter and amplify the electrical signals originating

from the battery during the quasi-static tests. The circuit consists of a preamplifier, a high-pass filter, and a differential amplifier. The preamplifier provides a better impedance matching between the battery and the input of the integrated circuit INA129P that implements the differential amplifier. This isolation prevents the battery's DC voltage component from saturating the differential amplifier.

As shown in Figure 5, the preamplifier consists of an arrangement around an N-type metal oxide field effect transistor (MOSFET) 2N7000, configured in a similar self-polarisation topology widely used with junction field effect transistor amplifiers. As depicted in Figure 5, this circuit was designed to provide the output voltages V_0^+ and V_0^-, which are two amplified versions of the input voltage V_{in}. This circuit combines a common-drain amplifier and a common source amplifier with resistive source degeneration. Thus, the output voltages V_0^+ and V_0^- of the preamplifier are respectively given by

$$V_0^+ = +\frac{g_m R_s}{1 + g_m R_s} V_{in}, \tag{1}$$

and

$$V_0^- = -\frac{g_m R_d}{1 + g_m R_s} V_{in}, \tag{2}$$

where g_m is the transconductance of the MOSFET. The variables R_d and R_s represent the resistances connected to the drain and source of the MOSFET , respectively. The differential voltage at the output of the preamplifier is given by

$$\begin{aligned} \Delta V_{pre} &= V_0^- - V_0^+ \\ &= -\frac{g_m}{1 + g_m R_s}(R_d + R_s) \times V_{in}. \end{aligned} \tag{3}$$

Since $R = R_s = R_d = 3.9\,\text{k}\Omega$, the differential voltage at the output of the preamplifier is then given by

$$\begin{aligned} \Delta V_{pre} = V_o^- - V_0^+ &= -\frac{2g_m R}{1 + g_m R} \times V_{in} \\ &= -\frac{7800 g_m}{1 + 3900 g_m} \times V_{in}. \end{aligned} \tag{4}$$

The measurements revealed a gain ($G_1 = \Delta V_{pre}/V_{in}$) of $G_1 \approx 1.5$ (or $G_{1,dB} = 3.5\,\text{dB}$). A differential high-pass filter with a very small near equal to zero lower cutoff frequency f_L was added after the preamplifier to eliminate the DC components of V_0^- and V_0^+ to prevent the saturation of the differential amplifier. The high-pass filter is first-order and presents the following transfer function

$$H(f) = \frac{j\left(\frac{f}{f_L}\right)}{1 + j\left(\frac{f}{f_L}\right)}, \tag{5}$$

where $f_L = 1/(2\pi R_2 C)$ is the lower cutoff frequency. This frequency is equal to $f_L = 0.07\,\text{Hz}$, e.g., as expected and designed, it is almost equal to the DC component,
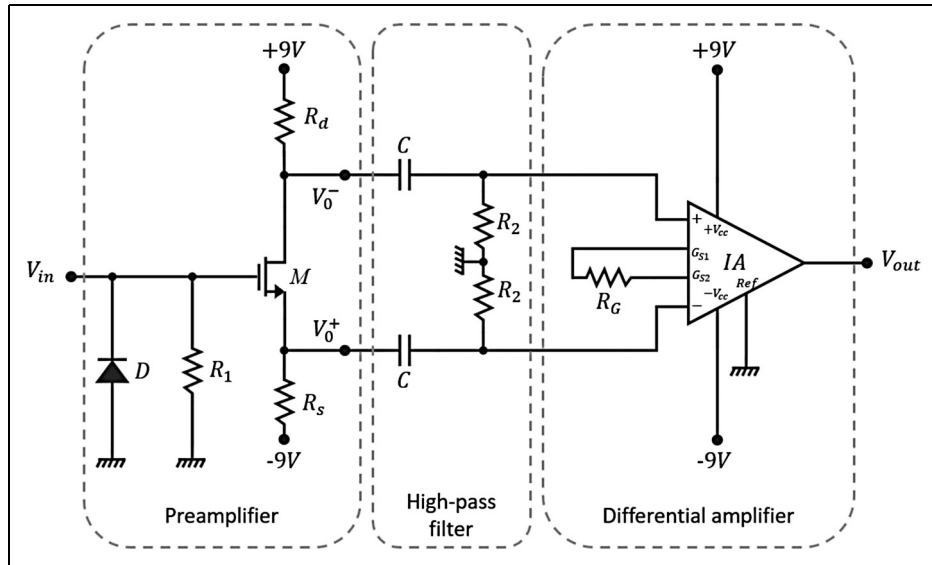
Figure 5. Schematic representation of the electronic circuit used to filter and amplify the AC signal coming from the battery and the respective constitutive blocks. In this circuit, the components are D (diode 1N4148), M (MOSFET 2N7000), IA (INA129P), $R_1 = 1\,M\Omega$, $R_2 = 4.7\,M\Omega$, $R_s = R_d = 3.9\,k\Omega$, $R_G \geq 1.6\,K\Omega$ (in series with a potentiometer), $C = 470\,nF$. Pins G_{s1} and G_{s2} are for gain settings purposes.
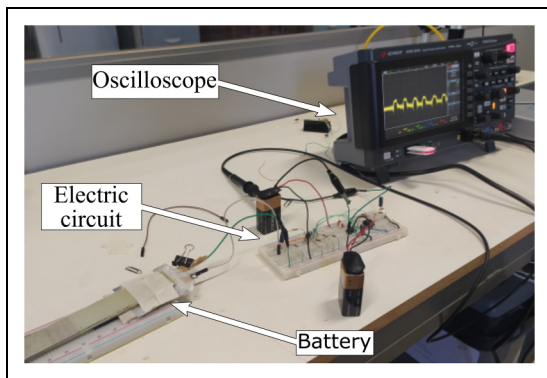

Figure 6. Experimental setup used when manual force is applied to the battery. The oscilloscope monitors the signal from the battery. The battery is positioned between two flat surfaces to ensure an even load distribution.

serving the purpose of cutting the 0 Hz and letting the remaining frequencies pass to the differential amplifier. The instrumentation amplifier model INA129P serves two purposes. First, the differential amplifier converts the voltage ΔV_{pre}^* (the filtered version from ΔV_{pre}) from the differential form into a voltage V_{out} with single-ended form. Second, the differential amplifier provides an additional gain G_2. The integrated circuit used to implement the differential amplification features low noise characteristics $(10\,nV/(Hz)^{1/2})$. The gain G_2 provided by the INA129P can be programmed using an external resistor $R_G[K\Omega]$ between the terminals G_{s1} and G_{s2} and is given by

$$G_2 = \frac{1 + 49.4}{R_g}. \tag{6}$$

Therefore, $R_G[K\Omega]$ was selected to be at least higher than 1.6 kΩ (e.g. $R_G \geq 1.6k\Omega$). This limits the gain of the

differential amplifier to $G \approx 31.9$ (or $G_{2,dB} = 30.1\,dB$) to limit the overall gain to $G = G_1 G_2 \approx 48$ (or $G_{dB} = 33.6\,dB$). This is achieved with a resistor of 1.6 kΩ in series with a potentiometer in series. This circuit is supplied by two external 9 V batteries and is placed between the battery and the oscilloscope to improve the sensitivity.

For the dynamic tests, a passive circuit is used, composed solely of capacitors, without any additional amplification or filters. This approach allows for a reduction in the DC passing through the capacitor, while still transferring the AC component to the data acquisition system.

Results and discussion

Quasi-Static results

Regarding the static tests, the aim is to assess the variation in the voltage of the battery due to a quasi-static load. In this proof-of-concept study, the intent is to analyse the results qualitatively. This approach demonstrated that the batteries generate a voltage difference when mechanically disturbed, proving their potential practicality as a sensor for damage monitoring applications.

In the initial tests, the load is manually applied to the battery. In this scenario, the battery produces a signal when subjected to a load, and this signal travels through the electrical circuit before being detected by the oscilloscope. Figure 6 depicts the complete experimental setup of the battery's static tests. Positioning the battery between two flat surfaces ensures even load distribution.

Initially, a very light pressure is applied to the battery to evaluate the noise level in the generated signal and assess the battery's sensitivity. Figure 7 shows a result of the electrical voltage on the battery by the time when
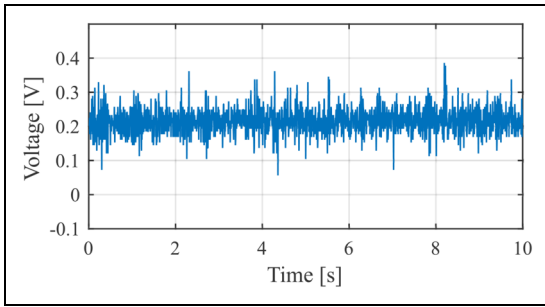
Figure 7. Variation in the electrical voltage of the battery when subjected to a light manual pressure: Dominant presence of noise in the obtained signal.

subjected to this light pressure. One observes only noise generated by the battery, and this behaviour occurs both for the undisturbed battery and when slight finger pressure is applied. Therefore, it is not possible to draw any definitive conclusions after these tests.

Subsequently, a more substantial load was manually applied to the battery. Here, the objective was to apply a manual load in a quasi-static, almost cyclical manner to assess if the battery consistently generates a difference in the signal in response to the applied load. Three repetitions of the tests were conducted using the same battery. In the first two tests, the battery was subjected to quasi-periodic but intermittent pressure. In the third test, the battery was subjected to quasi-periodic pressure, with intervals between successive load applications.

Figure 8 shows the results obtained, in which a substantial variation in the electrical potential of the battery is seen, significantly exceeding the signal noise. Applying the load in a quasi-periodic manner produced this dynamic response of the battery due to the mechanical stimuli. Given the piezoelectric nature of the battery, one would expect this response, as piezoelectric materials generate a potential difference when subjected to a deformation gradient. It is important to note that the pattern of the electrical signal generated by the battery when subjected to the application of cyclical loads precisely follows the pattern of the applied loads.

Hence, based on the preliminary results, it is confirmed that the battery exhibits piezoelectric behaviour. However, the significant noise level poses a challenge, as low loading levels might result in potential differences lower than the noise level, rendering an accurate assessment of its behaviour unfeasible.

The next analysis involves investigating the potential difference generated by the battery when a weight is applied to it. In this context, the weight is employed to maintain a consistent load on the battery. This approach enables a more controlled examination of the potential difference generated by the battery before, during, and after the placement of the mass. It is important to highlight that the aim is to qualitatively understand the behaviour of the battery under a consistent loading condition, such as load pressure. Hence, this test can be understood as a proof of concept.
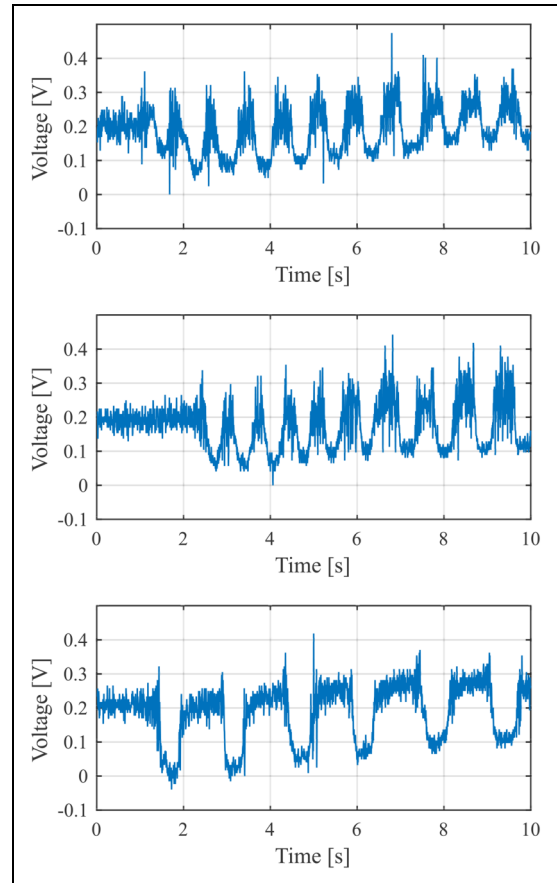

Figure 8. Variation in the electrical voltage of the battery from three different tests when subjected to manual cyclical pressure. The battery response follows the pattern of the load application.

Figure 9 shows the experimental setup of the tests. The battery is positioned between two fibre-glass composite plates to ensure an even contact surface. During the tests, the oscilloscope records the difference in the voltage of the battery before and after the positioning of the weight. The mass is positioned on the battery both abruptly and slowly, and each test is repeated three times.

Figure 10(a) depicts the change in electrical voltage observed during three subsequent static tests after setting a known metal weight abruptly on the battery. One consistently observes a peak voltage at around 6 s from the beginning of the test, which is approximately the time of application of the load, likely caused by the motion of the weight application (response to the mechanical impulse of a load pressure). Additionally, one can also note the difference in signal amplitude between the regions before and after the load application. This effect confirms the battery deformation and internal generation of an electrical potential difference upon mechanical loading. While this test is qualitative rather than quantitative, one can suggest that the battery has the theoretical potential to serve as a damage sensor detector, because, in this case, the structure deformation will change with the presence of the damage. Then, the deformation of the battery will change as well. Hence, by measuring
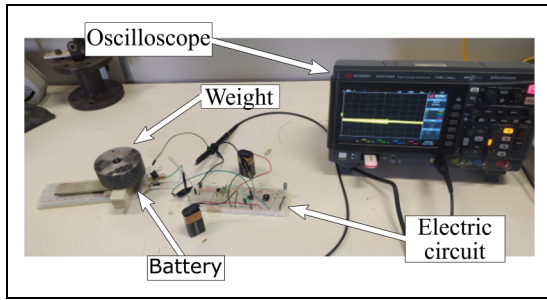
Figure 9. Experimental setup used when a metallic weight is placed on the battery to simulate a load pressure, and the behaviour of the battery is monitored on the oscilloscope. The battery is positioned between glass-fibre beams to ensure an even load distribution.

the evolution of the electrical potential difference in the battery, we can monitor those structural changes.

To reduce the pronounced effect of the mechanical impulse, the same test is repeated by applying the weight to the battery at a slower rate. Figure 10(b) depicts the results for three consecutive tests. As observed in the previous test, a peak voltage is seen at around 6 s after the test started, although lower than before. Additionally, a voltage difference in the signal is noticed before and after the load application, again less pronounced than before.

One observes that the battery shows a notably significant response when subjected to a variable load, i.e., the mechanical impulse. However, a definitive conclusion about the battery's behaviour before and after the load application is challenging due to the minimal potential difference in these two regions and the presence of considerable signal noise.

The qualitative tests indicate that using the batteries as damage sensors is possible. Some significant insights emerged from the analyses:

- In all the presented results, it is observed that the battery is strongly affected by noise. This effect is evident even in situations where the battery is not mechanically disturbed, as in Figure 7, and it is likely attributed to electromagnetic interference from the electrical network.
- When subjected to constant static loads, the battery shows a limited distinction in its electrical response between two different load scenarios. This behaviour is evident in Figure 10, where the responses are similar in regions with and without the stationary weight on the battery. Nevertheless, this is expected when considering the piezoelectric effect, as such materials are anticipated to generate a potential difference in response to variations in strain.
- The mechanical loading was applied as normal pressure on the battery's surface. However, in practical applications where the battery is attached to a structure, such as a plate or a beam, to operate as a damage sensor, the mechanical loading is usually transmitted from the structure to the battery as in-plane strains.

Consequently, the static tests performed did not fully validate the ability of the battery to respond to more general loading conditions, like flexure and torsion loadings.
- On the other hand, the results presented strongly suggest that the battery produces a potential difference, particularly under varying loads. This behaviour is highlighted in Figure 8, where the battery generates notable potential differences in response to a manually applied cyclic load, and in Figure 10, where the battery generates a significant potential difference due to the dynamic stimuli resulting from the mechanical impulse. This observation aligns with the piezoelectric effect, where changes in the strain field for this type of material lead to an electrical potential difference, and it is very promising for the proposed future application of the batteries as sensors. Therefore, the subsequent focus will be on the results of the dynamic tests.

Dynamic results

Regarding the dynamic tests, the objective is to evaluate the variation in electrical potential generated by the battery in response to dynamic stimuli. An AFG induces vibrations in the shaker that are transmitted to the battery. For this purpose, two types of signals are applied. The first signal is a sweep signal, as shown in Figure 11(a), where the AFG sweeps through all frequencies within a predetermined range over a specified time interval. The second signal is a constant-frequency sinusoidal signal, as shown in Figure 11(b).

In addition to evaluating the battery response under two different types of signals, two methods of attaching the battery to the coupling device are also employed. In the first boundary condition, shown in Figure 12(a), only one border of the protective polymeric part of the battery is clamped to the device, leaving the functional part of the battery entirely outside the rigid grip (BC 1). In the second boundary condition, shown in Figure 12(b), the functional part of the battery is entirely enclosed within the rigid grip (BC 2).

Table 1 summarises dynamic tests carried out on the batteries. Each test used two different batteries, and triplicates were performed for each case. For the constant-frequency sinusoidal signals, frequencies of 20, 30, and 50 Hz are considered, while for the sweep signal, the frequency range is 10–200 Hz in a 5 s time window. Additionally, an accelerometer is attached to the rigid grip for comparison purposes.

Figures 13 and 14 show the fast Fourier transform (FFT) results of the signals from battery 1 and battery 2, respectively, obtained for the constant frequencies and considering both boundary conditions. Additionally, the FFT from the accelerometer signal is shown for comparison. These results demonstrate the batteries can detect the operating frequencies of the shaker, as indicated by the prominent peaks at the frequencies of interest and their
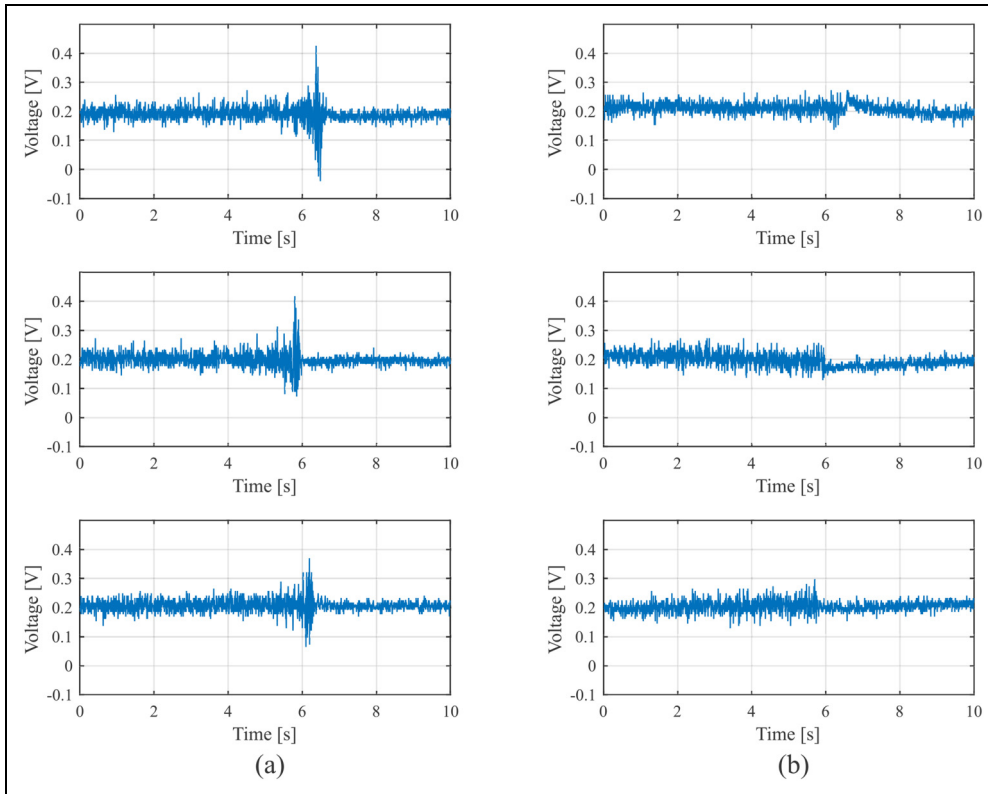
Figure 10. Variation in the electrical voltage of the battery due to a metallic weight placed on it from three different tests, depicting the effect of the mechanical impulse. The weight is positioned on the battery (a) abruptly and (b) slowly to simulate a load pressure.

Figure 11. Visualisation of the signals in the frequency generator that will be mechanically replicated by the shaker: (a) Sweep signal and (b) constant-frequency sinusoidal signal.

harmonics. The accelerometer signal is included for reference, showing peaks at the same frequencies.

Noteworthy, the batteries detect the operating frequencies for both analysed boundary conditions. This effect is relevant because the battery outside the rigid grip (BC 1) experiences significant bending, which is a similar scenario expected in applications involving the monitoring of structures. This result could be valuable in scenarios where these batteries are applied in SHM systems. Additionally, peaks at 60 Hz are observed in the battery signals for all cases. These peaks produced by the power line frequency imply the batteries are susceptible to electromagnetic interference. Thus, the noise source in all previously analysed cases is due to this interference from the electrical grid. Finally, the results consistently demonstrate that the battery signal at the frequency of

interest surpasses the signal due to noise, which is an important observation within the proposed context for the application of batteries as sensors. The only exception occurred with battery 2 under BC 1 at 50 Hz, where the interference signal amplitude exceeded that of the signal of interest.

A way to compare the level of the desired signal to the background noise signal is by using the signal-to-noise ratio (SNR), which for voltage measurement is given by

$$\text{SNR} = 20 \log\left(\frac{A_s}{A_n}\right) \quad [\text{dB}] \tag{7}$$

where A_s is the amplitude of the signal of interest and A_n is the amplitude of the noise signal. Table 2 shows the mean values of the SNR for all scenarios under constant
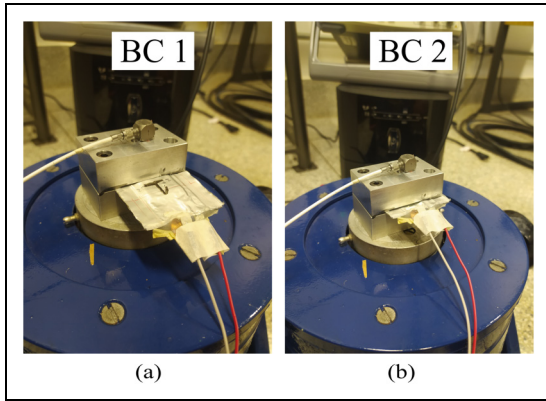
Figure 12. Different methods for attaching the battery to the rigid grip: (a) Functional area of the battery entirely outside the rigid grip (one border of the protective shell is fixed); (b) functional area of the battery completely enclosed within the rigid grip.

Table 1. Dynamic tests conducted on the batteries. In all cases, two distinct batteries are used, and three repetitions of each test are performed.

Test number	Boundary condition	Excitation	Frequency [Hz]
1	BC 1	Sinusoidal	20
2	BC 1	Sinusoidal	30
3	BC 1	Sinusoidal	50
4	BC 1	Sweep	10–200
5	BC 2	Sinusoidal	20
6	BC 2	Sinusoidal	30
7	BC 2	Sinusoidal	50
8	BC 2	Sweep	10–200

frequency excitations, alongside the standard deviation (SD) for each test.

By analysing the response of battery 1, it becomes apparent that, in all the analysed scenarios, the battery's signal at the frequency of interest is at least one order of magnitude larger than the interference signal amplitude. This underscores the battery's capability for potential use as a sensor. Furthermore, it is observed that there is a tendency for the battery's SNR to decrease at higher frequencies. This can be explained by the fact that the shaker generates larger amplitudes of movement at lower frequencies, consequently transferring greater deformations to the battery.

However, it is noticeable that the SNR varies between both batteries when examining the same scenario. In the analysis of battery 2, a consistently lower mean SNR is observed compared to battery 1 in all scenarios. Notably, in the case with boundary condition 1 under 50 Hz, the noise exceeds the signal of interest by 14 dB, i.e., almost an order of magnitude. This can be explained by the manual production of batteries, resulting in possible variations in both geometric and mechanical/electrical properties, consequently leading to differences in responses.

Figure 15 shows the FFT results of the signals of both batteries obtained for the sweep excitation and considering both boundary conditions. The FFT from the accelerometer is also shown for comparison. It is noticed that the most prominent peaks in the FFTs of the battery signals occur at multiples of 60 Hz, which, as previously discussed, are attributed to electromagnetic interference. In addition, it is challenging to derive a meaningful conclusion from this figure. There are some minor peaks at lower
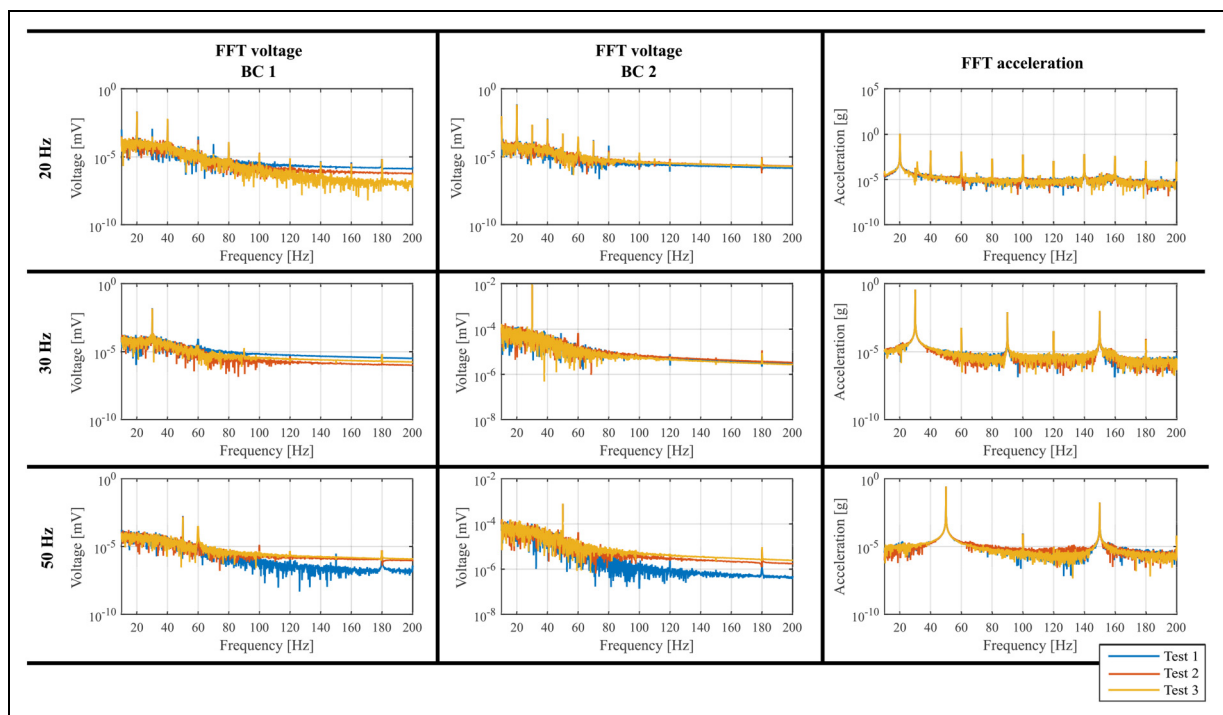

Figure 13. Fast Fourier transform (FFT) results obtained for battery 1 under constant frequencies, considering the boundary conditions, and comparison to the accelerometer under the same conditions.
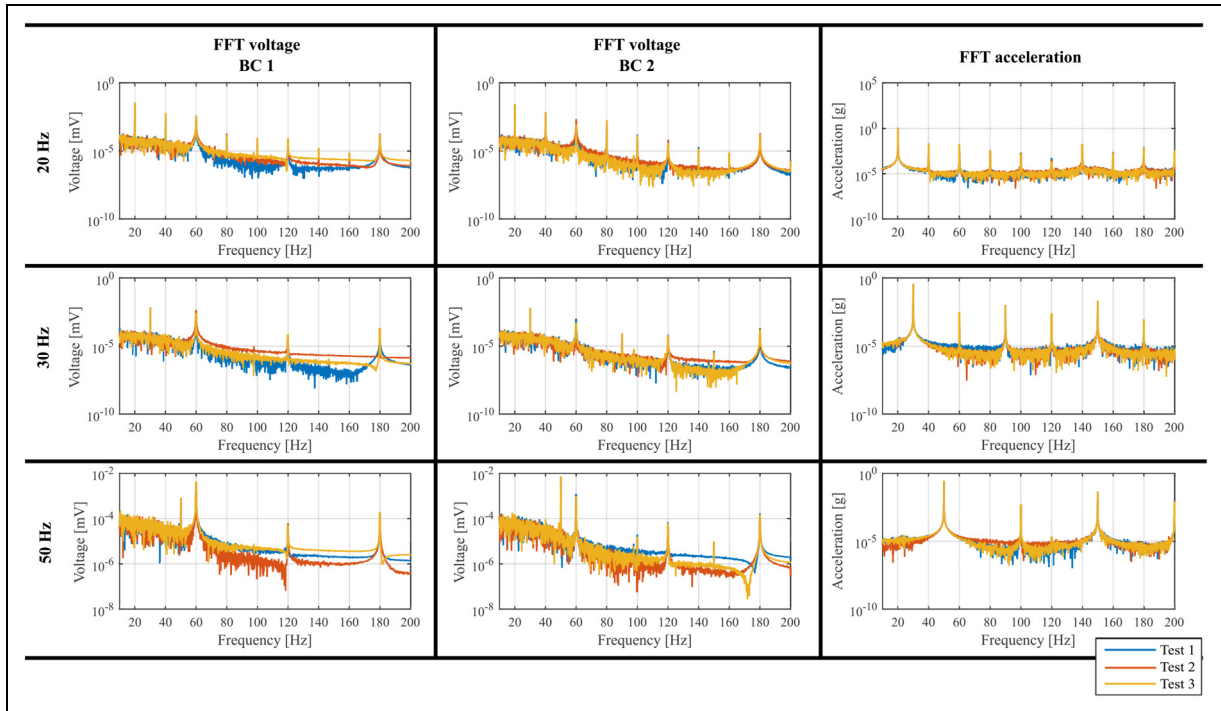
Figure 14. Fast Fourier transform (FFT) results obtained for battery 2 under constant frequencies, considering the boundary conditions, and comparison to the accelerometer under the same conditions.

frequencies, but the significant noise in the signal prevents any definitive conclusions. Since the shaker and rigid-grip system are considerably rigid, it is unlikely that any natural frequencies of this system will be excited during these analyses.

Furthermore, during the dynamic tests, an unusual behaviour of the shaker rigid-grip system was observed at frequencies between 20 and 25 Hz, resembling a system in resonance. These quasi-peaks are somewhat discerned in the accelerometer signals, but it is challenging to draw further conclusions solely by examining the battery signals.

Considering the outcomes of the dynamic tests, some considerations can be drawn:

- The dynamic tests provide strong evidence that batteries have the potential to work as damage sensors. When a sinusoidal input with constant frequencies is used to excite the battery, it is observed in the FFT that the signals from the batteries exhibit peak amplitudes that match the operating frequency of the shaker (and the harmonics), as well as the peak frequencies of the accelerometer.
- Upon analysing the SNRs of the signals obtained with constant frequency excitations, it was noted that the batteries produce signals with significantly higher amplitudes than the signal due to noise. Specifically for battery 1, the gain was at least one order of magnitude above the interference. This finding is promising because it suggests that the signal peaks in the frequency domain can be easily detected, supporting the idea that these batteries could be used as sensors in

Table 2. $\overline{\mathrm{SNR}}$ obtained with three subsequent tests and SD.

| Boundary condition | Freq. [Hz] | $\overline{\mathrm{SNR}} \pm$ SD [dB] | |
		Battery 1	Battery 2
BC 1	20	42.15 ± 5.63	19.16 ± 0.79
	30	51.03 ± 5.30	6.42 ± 2.17
	50	19.44 ± 7.97	-14.15 ± 0.72
BC 2	20	49.43 ± 3.39	27.66 ± 5.22
	30	49.55 ± 6.12	20.85 ± 4.89
	50	30.74 ± 5.20	18.15 ± 3.32

$\overline{\mathrm{SNR}}$: mean value of signal-to-noise ratio; SD: standard deviation.

the future. Battery 2, on the other hand, presented lower SNRs in comparison to battery 1, which might be attributed to deviations in the mechanical/electrical properties due to the manufacturing process.

- The noise level in the output signal of the batteries (voltage FFT) about the input peaks (acceleration FFT) captured by the accelerometer remains significantly high. This may suggest that the dynamic response of the battery is relatively weak and is substantially affected by electromagnetic noise. The development of specific electrical circuits might be necessary to improve the response signal of the battery. Additionally, one alternative way to mitigate electromagnetic interference would be applying a Notch filter to the signal, which is a feature commonly found in many data acquisition systems. The application of this filter around the frequency of 60 Hz would diminish the influence of the interference on
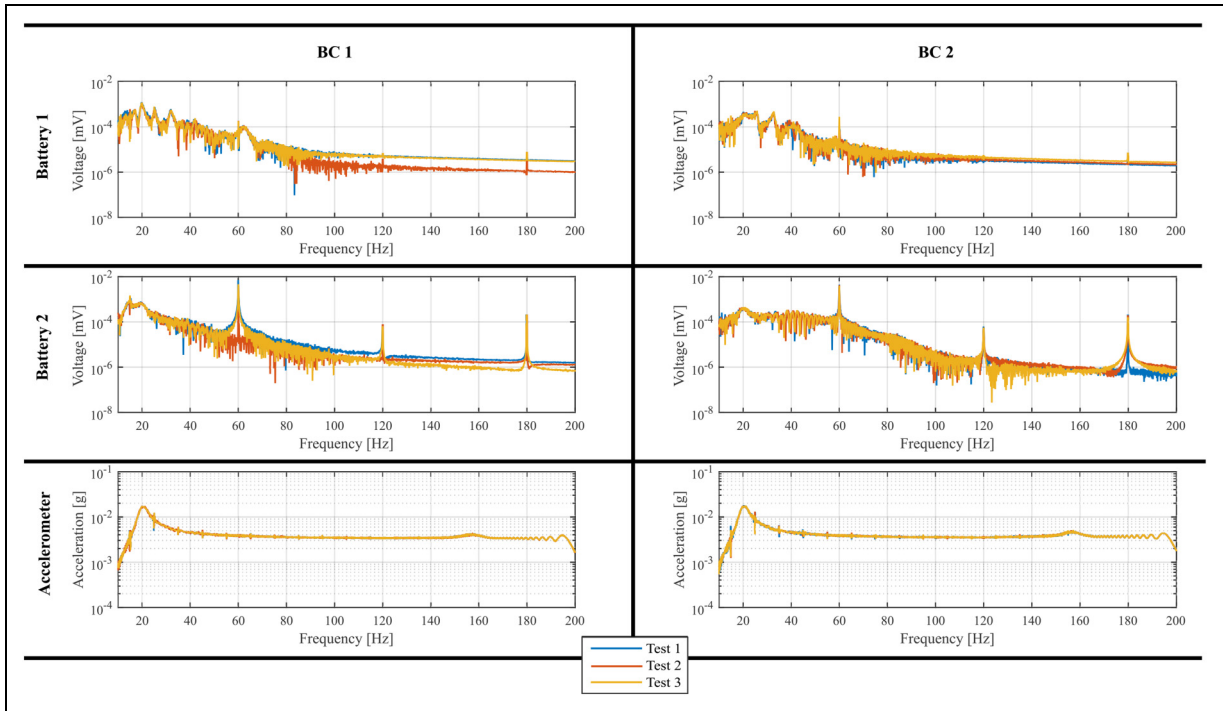
Figure 15. Fast Fourier transform (FFT) results obtained for both batteries under a sweep-like excitation, considering both boundary conditions, and comparison to the accelerometer under the same conditions.

the signal, thus improving the quality of the signal of interest, mainly for higher frequencies. This becomes particularly important when the case of battery 2 under BC1 at 50 Hz is considered, in which the interference signal exceeds the signal of interest. Implementing a Notch filter would improve the SNR of the battery, thus rendering the detection of the working frequency of the system clearer.

- The tests carried out with the battery under BC 1 are analogous to a cantilever beam configuration. Thus, the batteries are subjected to mechanical strains caused by bending, which closely approximates the loading conditions of a sensor monitoring a beam or plate structure in service.

Conclusion

In this study, the primary focus was exploring the potential use of a novel all-solid-state battery as a sensor, particularly in SHM applications. The battery, developed by the University of Porto in Portugal, is composed of a ferroelectric electrolyte based on sodium-ion and zinc (−) and copper (+) as the electrode pair. In this initial exploration of the potential use of these batteries as sensors, both quasi-static and dynamic tests were performed to assess how the battery signals respond to these mechanical stimuli.

In the quasi-static testing, a comparison between the signal generated by the undisturbed battery and the signal produced after positioning a stationary load revealed a minimal potential difference between the two scenarios. On the other hand, it was noted that the

battery induced a significant potential difference when subjected to dynamic stimuli. This observation occurred when placing weight on the battery, i.e., a mechanical impulse, and when the battery was manually pressed cyclically, simulating a load pressure on the battery.

In dynamic tests, the battery was subjected to excitations under constant sinusoidal frequencies and a sweep signal. When analysing the battery signal in the frequency domain, it was clearly observed that the battery is capable of generating a potential difference at the same base excitation frequency, considering the tests under constant sinusoidal frequencies. Furthermore, when examining the SNR of the battery in comparison to noise, one of the tested batteries demonstrated a signal that surpassed the noise in the analysed cases by at least one order of magnitude. This is particularly significant, as it indicates the battery's ability to produce a distinguishable signal from the interference.

Additionally, the battery was subjected to bending strains, which is a promising result when considering the applicability of this type of battery for damage monitoring, since this is a scenario close to what is expected in applications involving the monitoring of, for example, composite structures. The results hereby obtained further confirm the piezoelectric nature of the batteries and the potentiality of applying this novel technology as a sensing device. The proposed application of using batteries as sensors for future SHM applications has shown high promise mainly with the rigid control of the manufacturing process.

ORCID iDs

Bruno G Christoff https://orcid.org/0000-0003-2148-4596
Maísa M Maciel https://orcid.org/0000-0001-7227-0622
Volnei Tita https://orcid.org/0000-0002-8199-1162

References

1. Lewis NS. Powering the planet. *MRS Bull* 2007; 32: 808–820.
2. Larcher D and Tarascon JM. Towards greener and more sustainable batteries for electrical energy storage. *Nat Chem* 2015; 7: 19–29.
3. Armand M and Tarascon JM. Building better batteries. *Nature* 2008; 451: 652–657.
4. Carvalho Baptista M, Khalifa H, Araújo A et al. Giant polarization in quasi-adiabatic ferroelectric na+ electrolyte for solid-state energy harvesting and storage. *Adv Funct Mater* 2023; 33: 2212344.
5. Biemolt J, Jungbacker P, van Teijlingen T et al. Beyond lithium-based batteries. *Materials* 2020; 13: 425.
6. Danzi F, Valente M, Terlicka S et al. Sodium and potassium ion rich ferroelectric solid electrolytes for traditional and electrodeless structural batteries. *APL Mater* 2022; 10: 031111.
7. Kim Y, Seong WM and Manthiram A. Cobalt-free, high-nickel layered oxide cathodes for lithium-ion batteries: Progress, challenges, and perspectives. *Energy Storage Mater* 2021; 34: 250–259.
8. Zhu X, Savilov S, Ni J et al. Carbon nanoflakes as a promising anode for sodium-ion batteries. *Funct Mater Lett* 2018; 11: 1840011.
9. Wang Y, Song S, Xu C et al. Development of solid-state electrolytes for sodium-ion battery–a short review. *Nano Mater Sci* 2019; 1: 91–100.
10. Kim SW, Seo DH, Ma X et al. Electrode materials for rechargeable sodium-ion batteries: Potential alternatives to current lithium-ion batteries. *Adv Energy Mater* 2012; 2: 710–721.
11. Tarascon JM and Armand M. Issues and challenges facing rechargeable lithium batteries. *Nature* 2001; 414: 359–367.
12. Scrosati B. Recent advances in lithium ion battery materials. *Electrochim Acta* 2000; 45: 2461–2466.
13. Palacin MR. Recent advances in rechargeable battery materials: A chemist's perspective. *Chem Soc Rev* 2009; 38: 2565–2575.
14. Dunn B, Kamath H and Tarascon JM. Electrical energy storage for the grid: A battery of choices. *Science* 2011; 334: 928–935.
15. Danzi F, Salgado RM, Oliveira JE et al. Structural batteries: A review. *Molecules* 2021; 26: 2203.
16. Danzi F, Camanho PP and Braga MH. An all-solid-state coaxial structural battery using sodium-based electrolyte. *Molecules* 2021; 26: 5226.
17. Carrasco JM, Franquelo LG, Bialasiewicz JT et al. Power-electronic systems for the grid integration of renewable energy sources: A survey. *IEEE Trans Ind Electron* 2006; 53: 1002–1016.
18. Wu CW, Ren X, Zhou WX et al. Thermal stability and thermal conductivity of solid electrolytes. *APL Mater* 2022; 10: 040902.
19. Niazi M, Valente M and Braga MH. Structural batteries based on solid ferroelectric electrolytes. *Mater Proce* 2022; 8: 151.
20. El Moctar I, Ni Q, Bai Y et al. Hard carbon anode materials for sodium-ion batteries. *Funct Mater Lett* 2018; 11: 1830003.
21. Zhao C, Liu L, Qi X et al. Solid-state sodium batteries. *Adv Energy Mater* 2018; 8: 1703012.
22. Kim H, Kim H, Ding Z et al. Recent progress in electrode materials for sodium-ion batteries. *Adv Energy Mater* 2016; 6: 1600943.
23. Asp LE, Johansson M, Lindbergh G et al. Structural battery composites: a review. *Funct Compos Struct* 2019; 1: 042001.
24. Abdulkarem M, Samsudin K, Rokhani FZ et al. Wireless sensor network for structural health monitoring: A contemporary review of technologies, challenges, and future direction. *Struct Health Monit* 2020; 19: 693–735.
25. Di Rito G, Chiarelli MR and Luciano B. Dynamic modelling and experimental characterization of a self-powered structural health-monitoring system with mfc piezoelectric patches. *Sensors* 2020; 20: 950.
26. Xia H, Xia Y, Ye Y et al. Simultaneous wireless strain sensing and energy harvesting from multiple piezo-patches for structural health monitoring applications. *IEEE Trans Ind Electron* 2018; 66: 8235–8243.
27. Anton SR and Sodano HA. A review of power harvesting using piezoelectric materials (2003–2006). *Smart Mater Struct* 2007; 16: R1.
28. Park G, Rosing T, Todd MD et al. Energy harvesting for structural health monitoring sensor networks. *J Infrastruct Syst* 2008; 14: 64–79.
29. Hadas Z, Janak L and Smilek J. Virtual prototypes of energy harvesting systems for industrial applications. *Mech Syst Signal Process* 2018; 110: 152–164.
30. Christoff BG, Marques D and Carmo JP et al. On the strain-sensing capabilities of a novel all-solid-state sodium-based-electrolyte battery under vibration loads. *Mech Syst Signal Process* 2024; 215: 111390.